Journal of Energy Chemistry 25 (2016) 35–40

Contents lists available at ScienceDirect

Journal of Energy Chemistry

journal homepage: www.elsevier.com/locate/jechem

http://www.journals.elsevier.com/journal-of-energy-chemistry/

Biomass-derived activated carbon materials with plentiful heteroatoms for high-performance electrochemical capacitor electrodes

Xiangyang Zhou, Hongcheng Li, Juan Yang*

School of Metallurgy and Environment, Central South University, Changsha 410083, Hunan, China

ARTICLE INFO

Article history:
Received 14 July 2015
Revised 24 September 2015
Accepted 26 September 2015
Available online 21 November 2015

Keywords:
Electrochemical capacitor
Activated carbon
Soyabean
Heteroatoms

ABSTRACT

Activated carbons for electrochemical capacitor electrodes are prepared from soyabean using chemical activation with KOH. The pore size is easily controllable by changing the mass ratio between KOH and carbonized product. The as-prepared materials possess a large specific surface area, unique structure, well- developed hierarchical porosity and plentiful heteroatoms (mainly O and N). Thus resulted in its high specific capacitance, good rate capacity and cycling stability. Moreover, attributing to worldwide availability, renewable nature and low-cost, activated carbon prepared from soyabean has a good potential in energy conversion and storage devices.

1. Introduction

Electrochemical capacitor is a promising energy storage technology for applications where high power density and long-cycle life are required. Carbon materials have attracted intense interests as electrode materials for electrochemical capacitor, because of their high surface area, electrical conductivity, chemical stability and low cost [1]. Various carbonaceous materials, including carbon aerogels [2,3], carbon nanotubes [4,5], graphene [6,7], ordered mesoporous carbons (OMCs) [8,9] have been investigated as electrode materials of EDLC. However, the preparation for these carbons requires expensive and non-renewable raw materials, a lot of time and energy, and tedious preparation procedures [10]. By contrast, porous carbon materials derived from biomass are a potential choice for the construction of electrochemical capacitor electrodes owing to its worldwide availability, renewable nature and low-cost.

Up to now, many biomasses are converted into porous carbons, such as sunflower seed shell [10], broad beans [11], Rice husks [12] and collagen fiber [13,14]. However, the porous carbon derived from biomass usually suffers from limited capacitance. Incorporating heteroatoms (mainly N and O) into the carbon framework is an efficient approach for enhancing the capacitance performance of carbons [15]. The incorporated heteroatoms not only enhance the surface wettability of carbon material which would increase the surface area accessible to aqueous electrolyte, but also provide extra pseudo-capacitance [16–19]. In order to improve the charge storage ability, an efficient strategy is to carbonize heteroatom-containing precursors directly.

Herein, a heteroatom-enriched biomass, soyabean, has attracted our attention. Soyabean, as a renewable, abundant and environmentally friendly resource, is rich in carbon, nitrogen and oxygen elements, and thus can be carbonized into heteroatom-enriched carbon materials. We employ KOH as activated agent, and the pore structure can be easily tuned by changing the ration of KOH to carbon material. Symmetrical supercapacitors have been constructed and exhibited good electrochemical performance with a specific capacitance of 248.1 F/g at current density of 0.1 A/g and excellent cycle stability with 98.75% retention of the initial specific capacitance after 10,000 cycles at a current of 1 A/g.

2. Experimental

2.1. Preparation of materials

Soyabean powders received from bean milk factory was put into a quartz boat in a tubular furnace and then heated to 400 °C and maintained for 2 h under N_2 atmosphere (at a ramp of 5 °C/min). The obtained black carbonized products were impregnated with KOH solution and then dried in an electric oven at 120 °C for 12 h. The dried mixture was activated in a muffle furnace under a flow of N_2 gas at 750 °C and maintained for 2 h (at a ramp of 5 °C/min). After cooling under nitrogen flow, the resultant was thoroughly washed with 0.1 M HCl, followed by deionized water until pH = 6.5. And then the materials were dried at 60 °C in an electric oven. The product finally obtained was designated as AC-*X*, where *X* represents the mass ratio between KOH and carbonized product.

* Corresponding author. Tel/Fax: +86 0731 88836329.
E-mail address: j-yang@csu.edu.cn (J. Yang).

http://dx.doi.org/10.1016/j.jechem.2015.11.008
2095-4956/

2.2. Characterization

Field emission scanning electron microscopy (NOVA NANO SEM230, JAPAN) was used to characterize the materials. Chemical analysis was performed using an EDAX energy dispersive spectroscopy (EDS) system interfaced to the FESEM. X-ray photoelectron spectra (XPS) were recorded using an X-ray photoelectron spectrometer (K-Alpha 1063) with a monochromatic Al *Kα* X-ray source. Nitrogen adsorption and desorption isotherms were obtained at 77 K using a Micromeritics ASAP 2020 system. Specific surface areas were determined according to the Brunauer–Emmett–Teller (BET) method. The pore size distribution (PSD) plot was recorded from the adsorption branch of the isotherm based on the non-local density functional theory (NLDFT) method.

2.3. Electrode preparation and electrochemical measurements

The as-obtained materials was mixed with acetylene black and polytetrafluoroethylene (PTFE) at the mass ratio of 80:10:10, dried to subarid, rolled to slice with 0.1 mm in depth and cut into disks with 10 mm in diameter. The electrodes were transferred into a vacuum oven and dried overnight at 120 °C. The mass of each electrode was about 5–8 mg. A sandwich type cell was constructed from two electrodes, with similar weights, facing each other and separated non-woven paper. Standard 2025 coin cell design was utilized for the electrochemical tests employing 1 M H_2SO_4 as the electrolyte. Galvanostatic charging/discharging was carried out on LAND CT-2001A in the potential range of 0–0.9 V at different current densities of 0.1–20 A/g. Cyclic voltammetry (CV) measurements were performed at different constant scan rates (5–50 mV/s) from 0 to 0.9 V. The EIS was characterized at open circuit potential in the frequency range from 100 kHz to 0.01 Hz with the amplitude of 5 mV.

3. Results and discussion

The as-prepared materials are first characterized by SEM. As shown in Fig. 1(a), the sample AC-2 shows plenty cavities on surface. Fig. 1(b) shows the morphology of AC-3. It was obvious that the hole size of AC-3 is bigger than that of AC-2, which might attribute to the higher mass ratio of KOH and carbonized product. As shown in Fig. 1(c), the sample AC-4 is composed of fewer holes but micrometric curves within the texture. The sufficient amount of KOH etch carbon atom to make the holes disappear and curves remain. The specific architecture can provide electrolyte for nanoscale pore on these curves and therefore reduce the diffusion distances of charges to the interior.

Typical nitrogen adsorption–desorption isotherms at 77 K for the as-prepared carbon materials are depicted in Fig. 2(a). All the samples exhibit the type I isotherm, indicating that all samples are typical microporous carbon. It is obvious that the pore volume of AC-4 is much higher than those of AC-2 and AC-3. In addition, the isotherms of AC-4 show gradual increase at relative pressure $P/P_0 >$ 0.2, and a small hysteresis loop extending from $P/P_0 = 0.4$ to 0.9, indicating the co-existence of mesopores [19].

Pore size distributions obtained from the adsorption branch by the BJH model of the as-prepared porous carbon are shown in the Fig. 2(b). As shown in Fig. 2(b), all samples possess plentiful micropore size distribution (below 2 nm) but AC-4 also possesses considerable mesopores with pore size in the range of 2–5 nm. As demonstrated in the previous reports, the co-existence of small mesopores

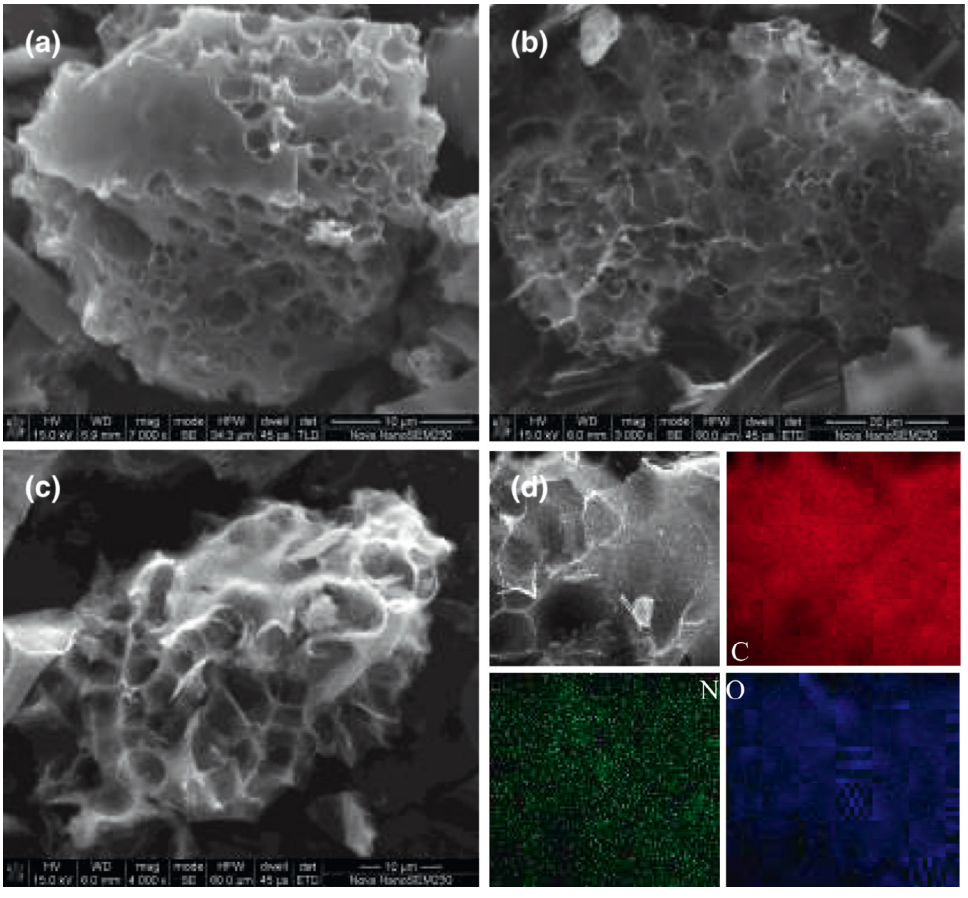

Fig. 1. (a–c) SEM images of AC-2, AC-3 and AC-4, (d) SEM images and corresponding elemental mapping images of AC-4.

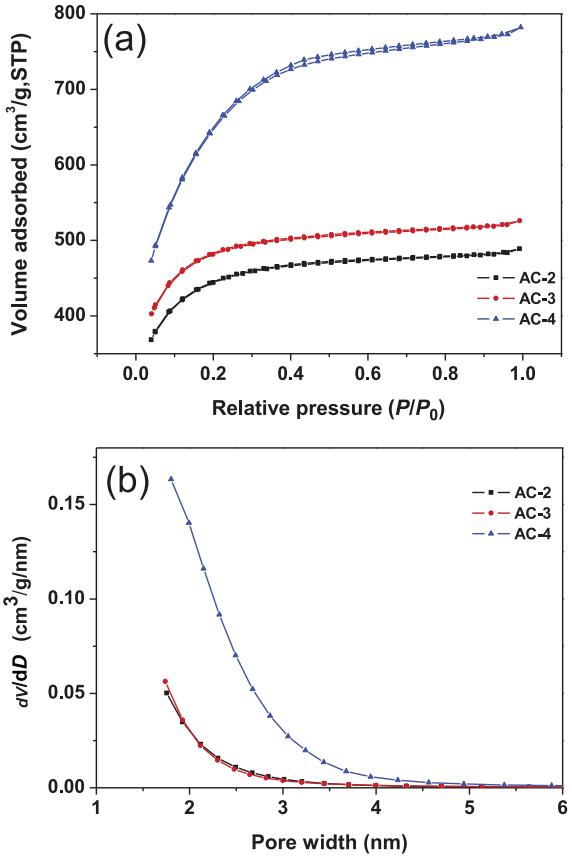

Fig. 2. (a) N_2 adsorption–desorption isotherms and (b) pore size distribution of AC.

Table 1. Physicochemical characterization of AC-2, AC-3 and AC-4.

Sample	Specific surface area (m^2/g)	Average pore diameter (nm)	Pore volume (cm^3/g)
AC-2	1561	1.93	0.756
AC-3	1694	1.95	0.8136
AC-4	2251	2.15	1.209

(2–4 nm) could provide low-resistance pathway for rapid ion diffusion at high current densities [20,21]. Table 1 provides details of the textural properties of the as-prepared materials. It is obvious that specific surface area, average pore diameter and pore volume are increasing with the alkali/carbon ratio. Wherein, the Specific surface area of AC-4 is as high as 2251 m^2/g, which is obviously a very positive factor to achieve a high electric double layer capacity. Pore size distribution is another important factor to affect the specific capacitance of a carbon electrode material [22,23]. As the chemical etching could broaden the range of pore size distribution, the pore size of the porous carbon materials is tunable by adjusting the alkali/carbon ratio. As shown in Table 1, the average pore sizes of AC-2, AC-3 and AC-4 are about 1.93, 1.95 and 2.15 nm, respectively. In addition, the bigger pore size of AC-4 is attributed to the creation of mesopores and macropores, which facilitate rapid ion transfer by serving as ion-buffering reservoirs and ion-transport pathways [24–26].

The surface chemical properties of the as-prepared materials are analyzed by X-ray photoelectron spectroscopy (XPS). Fig. 3(a) shows the survey scan spectrum of the AC-4 with apparent C 1*s*, N 1*s* and O 1*s* peaks. The as-prepared AC-4 possesses the presence of carbon, nitrogen and oxygen elements and the corresponding contents are 89.93, 1.69 and 8.38 at%, respectively. The element contents of all samples are present in Table 2. All samples have the similar content of

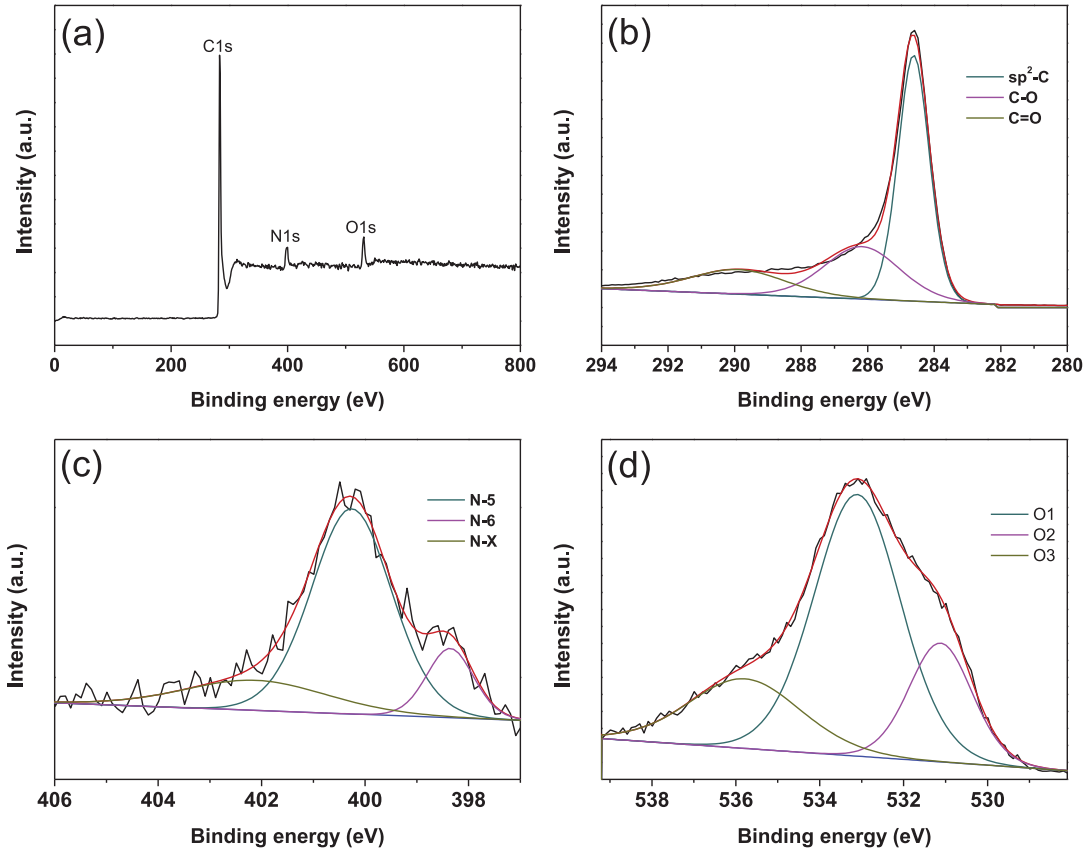

Fig. 3. (a) XPS survey spectra of AC-4, (b) C 1*s* XPS spectra, (c) N 1*s* XPS spectra and (d) O 1*s* XPS spectra.

Table 2. Element contents of AC-2, AC-3 and AC-4.

Sample	Element content (at%)		
	C	N	O
AC-2	91.21	1.71	7.08
AC-3	90.90	1.83	7.25
AC-4	89.93	1.69	8.38

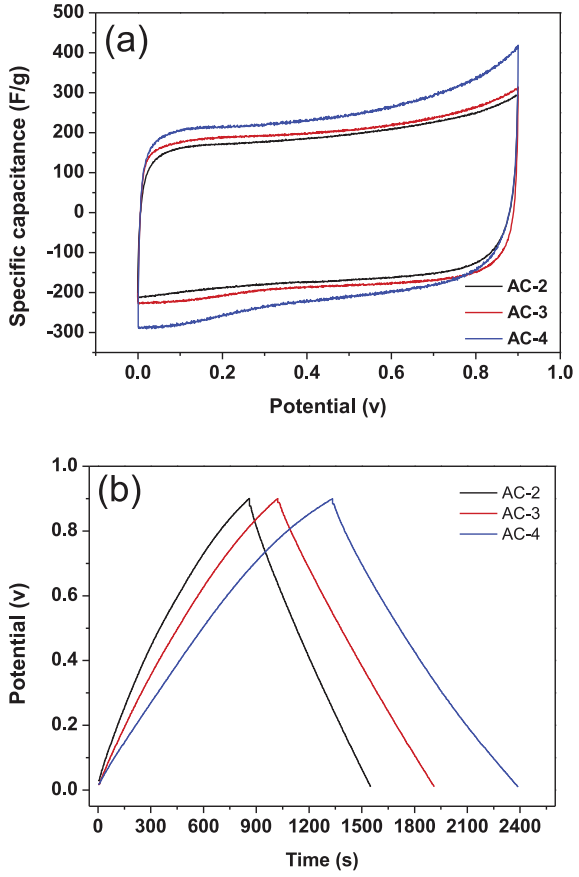

Fig. 4. (a) CV curves of AC at 2 mV/s, (b) galvanostatic charge–discharge curves of AC.

elements but the incorporating heteroatoms content of AC-4 is higher than those of AC-2 and AC-3. The C 1*s* peaks at 289.89, 286.17 and 284.62 eV are attributed to O=C, C–O and sp^2-C, respectively (Fig. 3b). The former two confirm the existence of oxygen functionalities. The N 1*s* peaks can be assigned to three types: N-X (pyridine-N-oxyde, 402.12 eV), N-5 (pyrrolic nitrogen, 400.26 eV) and N-6 (pyridinic nitrogen, 398.36 eV) (Fig. 3c). The O 1*s* peaks at 533.11 eV (O1) and 531.12 eV (O2) provide a further evidence for the existence of surface oxygen groups in the form of C–O and O=C (Fig. 3d). The O 1*s* peaks at 535.78 eV (O3) are corresponding to chemisorbed oxygen and/or water. As known, the presence of surface oxygen groups and nitrogen groups not only improve the hydrophilicity of carbon material which would increase the surface area accessible to aqueous electrolyte, but also provided extra pseudo-capacitance [16–18,27,28]. The mapping images (Fig. 1d) indicate that nitrogen and oxygen are homogeneously distributed in the carbon.

The capacitive performance of the as-prepared materials is studied using cyclic voltammetry (CV) and galvanostatic charge-discharge methods in a symmetrical two-electrode cell. As presented in Fig. 4(a), it can be seen that all CV curves exhibit an approximately rectangular, showing the double-layer capacitance behavior. It is obvious that the specific capacitance of AC-4 is much higher than those of AC-2 and AC-3. The galvanostatic charge–discharge curves at a current density of 0.1 A/g are shown in Fig. 4(b). The linear and symmetrical voltage-time curves demonstrate good electrochemical reversibility and coulombic efficiency. The specific capacitances of AC-2, AC-3 and AC-4 are estimated to be 163.6, 208.4 and 248.1 F/g at a current density of 0.1 A/g, respectively, which are in good agreement with the CV test (Fig. 4a). As expected, AC-4 apparently indicates much higher specific capacitance than those of AC-2 and AC-3. The superior capacitance of AC-4 could be reasonably ascribed to its high specific surface area, large pore volume, reasonable pore size distribution, as well as the content of oxygen groups and nitrogen groups.

Table 3. Comparison between AC-4 and HPC.

Sample	Specific surface area (m^2/g)	Pore volume (cm^3/g)	Specific capacitance (F/g)
AC-4	2250	1.21	248
HPC	2860	1.63	130

To investigate the attribution of N and O heteroatoms to the performance of the capacitor, a comparison is made between AC-4 and a high porosity carbon (HPC) derived from mesophase pitch in previous report [29]. HPC has been prepared using chemical activation with KOH and applied as electrode for electrochemical capacitor. Its electrochemical performance was tested in the same way that employing 1 M H_2SO_4 as electrolyte and choosing 0–0.9 V as the potential range. As can be seen in Table 3, HPC has a high BET specific surface area of 2860 m^2/g and a capacitance of 130 F/g. Although the porosity of AC-4 is less developed than that of HPC, the capacitance of AC-4 is nearly twice that of HPC. The enhancing capacitance of AC-4 could be ascribed to the existence of incorporating heteroatoms, which can increase the electrical conductivity, wettability, and contribute to a pseudocapacitive effect [9,11,30,31].

Fig. 5(a) shows the CV curves of AC-4 electrode at scan rates of 2, 5, 10, 20, 30, 40 and 50 mV/s. It is noticeable that the materials exhibit excellent electrochemical behavior in a wide range of scan rates. Fig. 5(b) shows the galvanostatic charge–discharge curves of the assembled symmetrical supercapacitors at different current densities. The resulting porous carbon electrode materials at current densities of 0.1, 0.2, 0.5 and 1A/g, show specific capacitance of 248.1, 245.6, 235 and 229.5 F/g, respectively. Fig. 5(c) shows the variation of the specific capacitance at different current densities. The as-prepared AC-4 supercapacitor exhibits a good rate capability (56.7% capacity retention from 0.1 to 20 A/g), which could be due to the unique hierarchically porous structure for providing fine diffusion pathways for electrolyte. Fig. 5(d) shows the stability of AC-4 during charge–discharge cycling at a current density of 1 A/g. The capacitance retention is 98.75% after 10,000 cycles, showing good electrochemical stability.

The electrochemical impedance spectra (EIS) of the porous carbon electrodes are depicted in Fig. 6. As shown in Fig. 6, all the impedance spectra of the samples are almost similar, which contain a semicircle in the high frequency region and a linear part at the low frequency region. The depressed semicircle represents the charge transfer resistance at the electrode/electrolyte interface. The vertical line indicates a capacitive behavior, on behalf of the ion diffusion in the electrode. AC-4 shows a more vertical line at low frequency than the other two carbon samples, indicating a nearly ideal capacitive behavior and low diffusion resistance of electrolyte ions in the electrode material [32]. In the high frequency region, the real axis intercept are 0.65, 0.6 and 0.5 Ω for AC-2, AC-3 and AC-4, respectively, indicating that AC-4 has smaller solution resistance including the ionic resistance of the electrolyte, intrinsic resistance of the substrate, and contact resistance. The radius of semicircle for AC-4 is shorter than that of the AC-3, but longer than that of the AC-2. This might be due to unique hierarchically porous structure of AC-4 and poor pore architecture of AC-2.

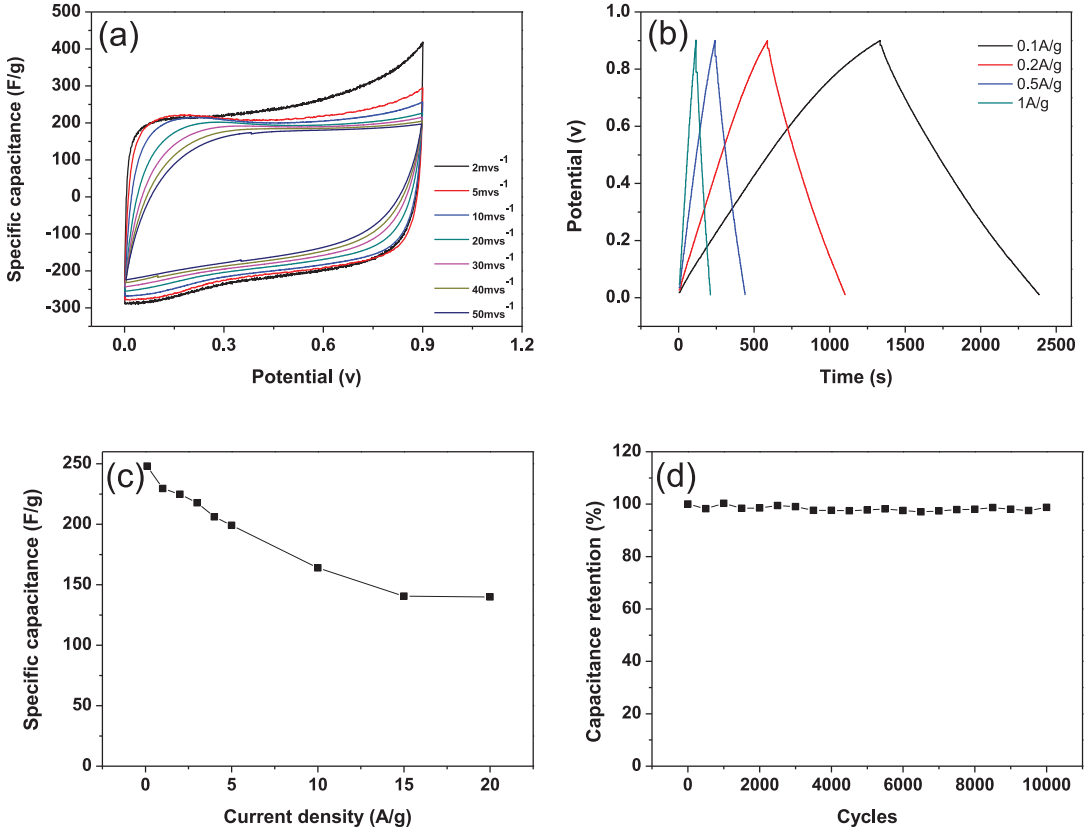

Fig. 5. (a) CV curves of AC-4 at different scan rates, (b) galvanostatic charge–discharge curves of AC-4 at different current densities, (c) specific capacitance of AC-4 at different current densities, (d) cycle stability of AC-4 at current density of 1 A/g.

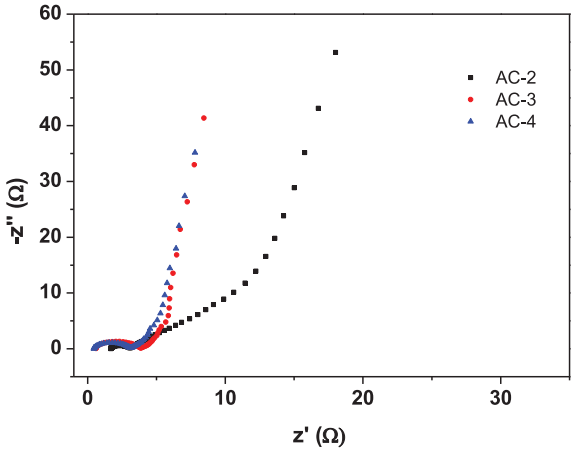

Fig. 6. Nyquist plots of ACs.

4. Conclusions

A kind of porous carbon material containing plentiful heteroatoms (mainly O and N) have been successfully prepared using Soyabean as raw materials and applied as electrode material for electrochemical capacitors. The pore size of the porous carbon materials is tunable by adjusting the alkali/carbon ratio. The sample AC-4 possesses largest specific surface area of 2251 m^2/g and the highest capacitance value of 248 F/g at 0.1 A/g. What's more, it has good rate capacity (56.7% capacity retention from 0.1 to 20 A/g) and excellent cycling stability (98.75% capacity retention after 10,000 cycles). Its good electrochemical performance can be attributed to large specific surface area, unique structure, well developed hierarchical porosity and plentiful heteroatoms. The porous carbon materials prepared from widely available raw material by low-cost method have a good potential in energy conversion and storage devices.

References

[1] Y. Zhai, Y. Dou, D. Zhao, P.F. Fulvio, R.T. Mayes, S. Dai, Adv. Mater. 23 (42) (2011) 4828–4850.
[2] Z. Zapata-Benabithe, F. Carrasco-Marín, C. Moreno-Castilla, J. Power Sour. 219 (2012) 80–88.
[3] D. Liu, J. Shen, N. Liu, H. Yang, A. Du, Electrochima Acta 89 (2013) 571–576.
[4] M.H. Ervin, B.S. Miller, B. Hanrahan, B. Mailly, T. Palacios, Electrochima Acta 65 (2012) 37–43.
[5] D.N. Futaba, K. Hata, T. Yamada, T. Hiraoka, Y. Hayamizu, Y. Kakudate, O. Tanaike, H. Hatori, M. Yumura, S. Iijima, Nat. Mater. 5 (12) (2006) 987–994.
[6] S. Murali, J.R. Potts, S. Stoller, J. Park, M.D. Stoller, L.L. Zhang, Y. Zhu, R.S. Ruoff, Carbon 50 (10) (2012) 3482–3485.
[7] J. Chen, C. Li, G. Shi, J. Phys. Chem. Lett. 4 (8) (2013) 1244–1253.
[8] S. Feng, W. Li, J. Wang, Y. Song, A.A. Elzatahry, Y. Xia, D. Zhao, Nanoscale 6 (24) (2014) 14657–14661.
[9] J. Wei, D. Zhou, Z. Sun, Y. Deng, Y. Xia, D. Zhao, Adv. Funct. Mater. 23 (18) (2013) 2322–2328.
[10] X. Li, W. Xing, S. Zhuo, J. Zhou, F. Li, S.-Z. Qiao, G.-Q. Lu, Bioresour. Technol. 102 (2) (2011) 1118–1123.
[11] G. Xu, J. Han, B. Ding, P. Nie, J. Pan, H. Dou, H. Li, X. Zhang, Green Chem. 17 (2015) 1668–1674.
[12] Y. Gao, L. Li, Y. Jin, Y. Wang, C. Yuan, Y. Wei, G. Chen, J. Ge, H. Lu, Appl. Energy 153 (2015) 41–47.
[13] D. Deng, X. Liao, B. Shi, ChemSusChem 1 (4) (2008) 298–301.
[14] D. Deng, H. Wu, X. Liao, B. Shi, Microporous Mesoporous Mater. 116 (1) (2008) 705–709.
[15] C. Ruan, K. Ai, L. Lu, RSC Adv. 4 (58) (2014) 30887–30895.
[16] H. Nishihara, T. Kyotani, Adv. Mater. 24 (33) (2012) 4473–4498.
[17] W. Li, F. Zhang, Y. Dou, Z. Wu, H. Liu, X. Qian, D. Gu, Y. Xia, B. Tu, D. Zhao, Adv. Energy Mater. 1 (3) (2011) 382–386.
[18] E. Iyyamperumal, S. Wang, L. Dai, ACS Nano 6 (6) (2012) 5259–5265.
[19] Y. Fan, P.-F. Liu, Z.-J. Yang, T.-W. Jiang, K.-L. Yao, R. Han, X.-X. Huo, Y.-Y. Xiong, Electrochima Acta 163 (2015) 140–148.
[20] P. Simon, Y. Gogotsi, Nat. Mater. 7 (11) (2008) 845–854.

[21] M. Rose, Y. Korenblit, E. Kockrick, L. Borchardt, M. Oschatz, S. Kaskel, G. Yushin, Small 7 (8) (2011) 1108–1117.
[22] J. Chmiola, G. Yushin, R. Dash, Y. Gogotsi, J. Power Sour. 158 (1) (2006) 765–772.
[23] J. Chmiola, G. Yushin, Y. Gogotsi, C. Portet, P. Simon, P.-L. Taberna, Science 313 (5794) (2006) 1760–1763.
[24] Y. Liang, F. Liang, D. Wu, Z. Li, F. Xu, R. Fu, Phys. Chem. Chem. Phys. 13 (19) (2011) 8852–8856.
[25] H. Zhong, F. Xu, Z. Li, R. Fu, D. Wu, Nanoscale 5 (11) (2013) 4678–4682.
[26] L. Wang, Y. Zheng, Q. Zhang, L. Zuo, S. Chen, S. Chen, H. Hou, Y. Song, RSC Adv. 4 (93) (2014) 51072–51079.
[27] L. Wei, G. Yushin, Nano Energy 1 (4) (2012) 552–565.
[28] S. Gao, Y. Chen, H. Fan, X. Wei, C. Hu, H. Luo, L. Qu, J. Mater. Chem. A 2 (10) (2014) 3317–3324.
[29] T.-C. Weng, H. Teng, J. Electrochem. Soc. 148 (4) (2001) A368–A373.
[30] H. Wang, J. Liu, K. Zhang, H. Peng, G. Li, Synth. Met. 203 (2015) 149–155.
[31] E. Raymundo-Piñero, F. Leroux, F. Béguin, Adv. Mater. 18 (14) (2006) 1877–1882.
[32] J. Wang, L. Shen, B. Ding, P. Nie, H. Deng, H. Dou, X. Zhang, RSC Adv. 4 (15) (2014) 7538–7544.